

## Lipid Organization of the Plasma Membrane

Helgi I. Ingólfsson,<sup>†</sup> Manuel N. Melo,<sup>†</sup> Floris J. van Eerden,<sup>†</sup> Clément Arnarez,<sup>†</sup> Cesar A. Lopez,<sup>†</sup> Tsjerk A. Wassenaar,<sup>†,‡</sup> Xavier Periole,<sup>†</sup> Alex H. de Vries,<sup>†</sup> D. Peter Tieleman,<sup>§</sup> and Siewert J. Marrink<sup>\*,†</sup>

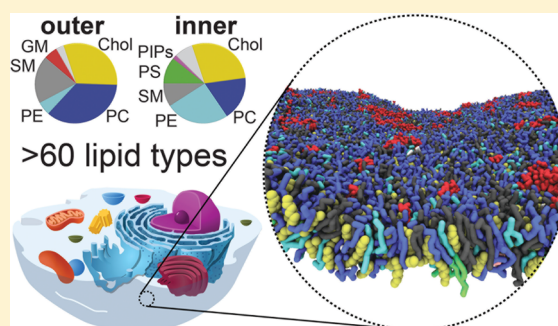
<sup>†</sup>Groningen Biomolecular Sciences and Biotechnology Institute and Zernike Institute for Advanced Materials, University of Groningen, Nijenborgh 7, 9747 AG Groningen, The Netherlands

<sup>‡</sup>Computational Biology, Department of Biology, University of Erlangen-Nürnberg, Staudtstr. 5, 91052 Erlangen, Germany

<sup>§</sup>Centre for Molecular Simulation and Department of Biological Sciences, University of Calgary, 2500 University Dr. NW, Calgary, Alberta T2N 1N4, Canada

### Supporting Information

**ABSTRACT:** The detailed organization of cellular membranes remains rather elusive. Based on large-scale molecular dynamics simulations, we provide a high-resolution view of the lipid organization of a plasma membrane at an unprecedented level of complexity. Our plasma membrane model consists of 63 different lipid species, combining 14 types of headgroups and 11 types of tails asymmetrically distributed across the two leaflets, closely mimicking an idealized mammalian plasma membrane. We observe an enrichment of cholesterol in the outer leaflet and a general non-ideal lateral mixing of the different lipid species. Transient domains with liquid-ordered character form and disappear on the microsecond time scale. These domains are coupled across the two membrane leaflets. In the outer leaflet, distinct nanodomains consisting of gangliosides are observed. Phosphoinositides show preferential clustering in the inner leaflet. Our data provide a key view on the lateral organization of lipids in one of life's fundamental structures, the cell membrane.



### INTRODUCTION

Cell membranes are complex assemblies of lipids and proteins that separate the cell interior from the outside environment. Despite the simple bilayer nature of the membrane, lipidomics studies have identified a tremendous variety of lipid species involved in its constitution. Typical plasma membranes (PM) contain hundreds of different lipids.<sup>1–3</sup> The lateral mixing of these components is presumably highly non-uniform.<sup>4,5</sup> In fact, plasma membranes are close to a miscibility critical point,<sup>6</sup> and large-scale phase separation can occur near physiological conditions.<sup>7,8</sup> This lateral segregation potential or “patchiness” of the membrane has important implications for many cellular processes, e.g., protein trafficking and aggregation, membrane fusion, and signal transduction. Changes in expression levels of individual lipid species have been implicated in many diseases including: cancers, diabetes, Alzheimer's disease, HIV entry, and atherosclerosis.<sup>9,10</sup> Despite recent progress,<sup>11,12</sup> *in vivo* characterization of the structural heterogeneity remains very challenging due to the high spatiotemporal resolution required to study fluctuating nanoscale assemblies of lipids and proteins in living cells.

To understand the driving forces governing the structural and dynamical organization of cellular membranes, computer simulation has become an indispensable tool. “Computational microscopy” can be considered a complement to traditional microscopy methods.<sup>13,14</sup> Notably, simulation studies of membranes are becoming increasingly sophisticated.<sup>15</sup> Never-

theless, membrane complexity is still limited to bilayers consisting of, at most, four or five lipid components.<sup>16–19</sup>

Here we developed a dynamic model of a realistic plasma membrane at near-atomic detail, containing more than 60 different lipids. As PM lipid composition varies significantly between different organisms and cell types and depends on the stage of the cell cycle as well as environmental factors,<sup>1,2</sup> the composition represents an average idealized mammalian plasma membrane, with phosphatidylcholines (PC), sphingomyelin (SM), and gangliosides (GM) predominantly in the outer leaflet and phosphatidylethanolamine (PE), phosphatidylserine (PS), and other charged lipids in the inner leaflet (Figure 1 and Tables S1–S2). Lipid tails range between fully saturated and polyunsaturated, with a larger fraction of unsaturated tails assigned to the inner leaflet (Figure 1 and Tables S1–S2). Eukaryotic plasma membranes also contain around 20–50% sterols;<sup>1,20</sup> we included 30 mol % cholesterol in our PM model. To make the simulations computationally feasible, we used a coarse-grained (CG) model in which small groups of atoms (3–4 heavy atoms) are united into chemical entities.<sup>21</sup> The combined headgroups and lipid acyl chains represented in our PM model resulted in 63 different lipid species that, to our knowledge, is by an order of magnitude the most complex bilayer composition that has been simulated to date.

Received: July 31, 2014

Published: September 17, 2014

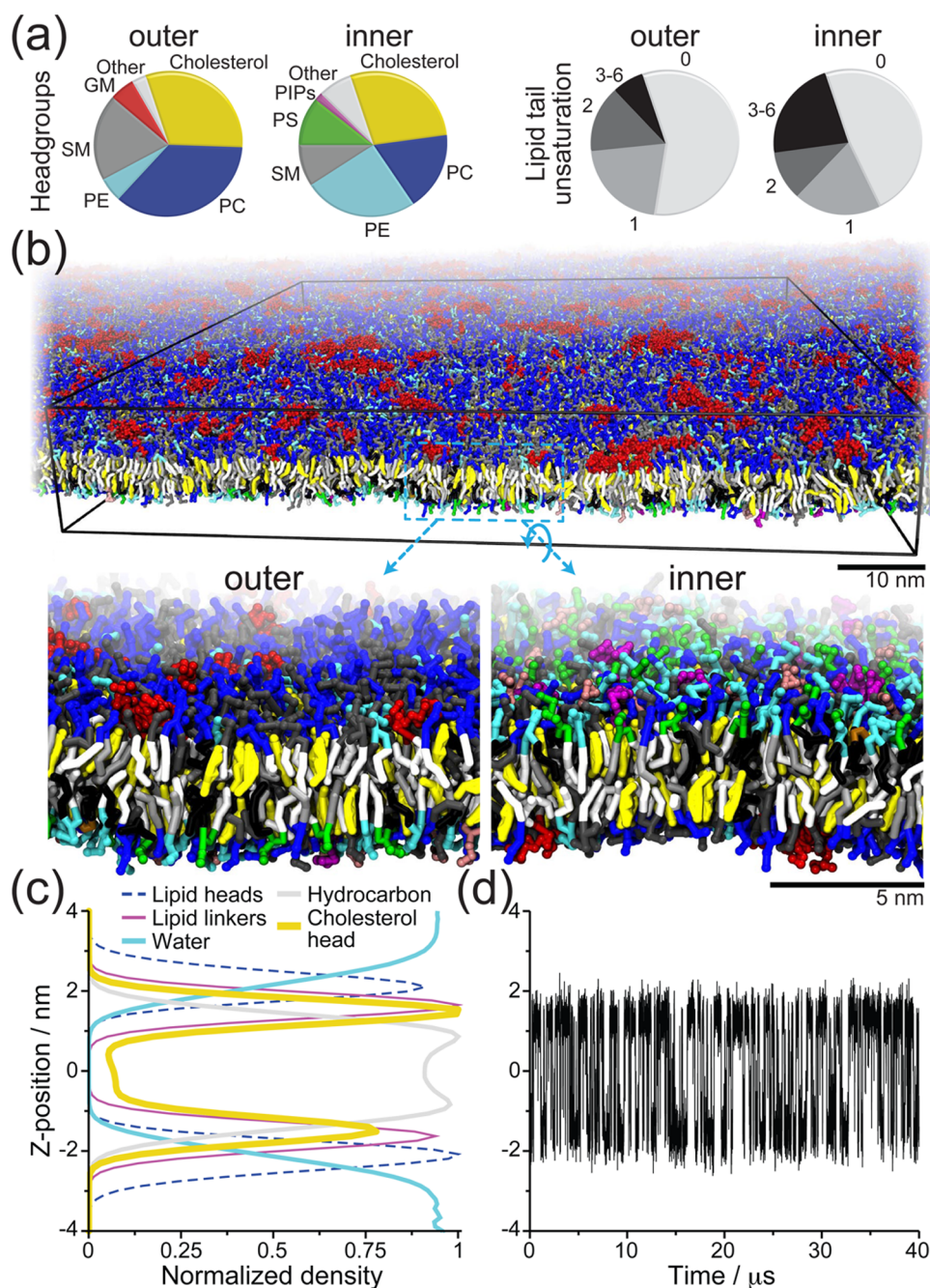


**Figure 1.** Plasma membrane lipid and cholesterol distribution. (a) Pie charts showing the distribution of the main lipid headgroups and the levels of tail unsaturation in the inner and outer leaflets. (b) A snapshot of the plasma membrane after 40  $\mu$ s of simulation viewed from the outer leaflet. Underneath are two zoomed in cross sections viewed from the outer and inner PM side, respectively. Cholesterols are colored yellow, lipid headgroups are colored by type (PC, blue; SM, gray; PE, cyan; GM, red; PIPs, magenta; PI, pink; PS, green; PA, white; CE, ice blue; DG, brown; LPC, orange), and tails by number of unsaturated bonds (0, white; 1, light gray; 2, dark gray; 3–6, black). (c) The PMs density profile across the membrane, averaged from 38 to 40  $\mu$ s, shows the asymmetric cholesterol distribution; 54% in the outer vs 46% in the inner leaflet. (d) The Z-position, with respect to the bilayer center, of the polar head of a cholesterol molecule, demonstrating the fast cholesterol flip-flop rate between the leaflets, see Methods in Supporting Information for analysis and rates.

Determining the lateral distribution of lipids and its influence on membrane protein function is one of the key challenges in cell biology and is crucial for understanding eukaryotic life. Our study provides a detailed view of lipid organization in the PM at near-atomic resolution, across length scales from individual lipids to 70 nm and time scales ranging from nano- to microseconds. Our results provide insight on the much debated trans-leaflet distribution of cholesterol, the extent of nanoscale

heterogeneity in the membrane, and preferential clustering of lipid types.

## METHODS

**Bilayer Composition.** All major lipid headgroups known to reside in mammalian PMs were included, and their distribution and molar ratios were set to fit an idealized PM.<sup>1,2,22–24</sup> The charged species PS, phosphatidic acid (PA), phosphatidylinositol (PI), and the PI-phosphate, -bisphosphate, and -trisphosphate (PIPs) were placed in

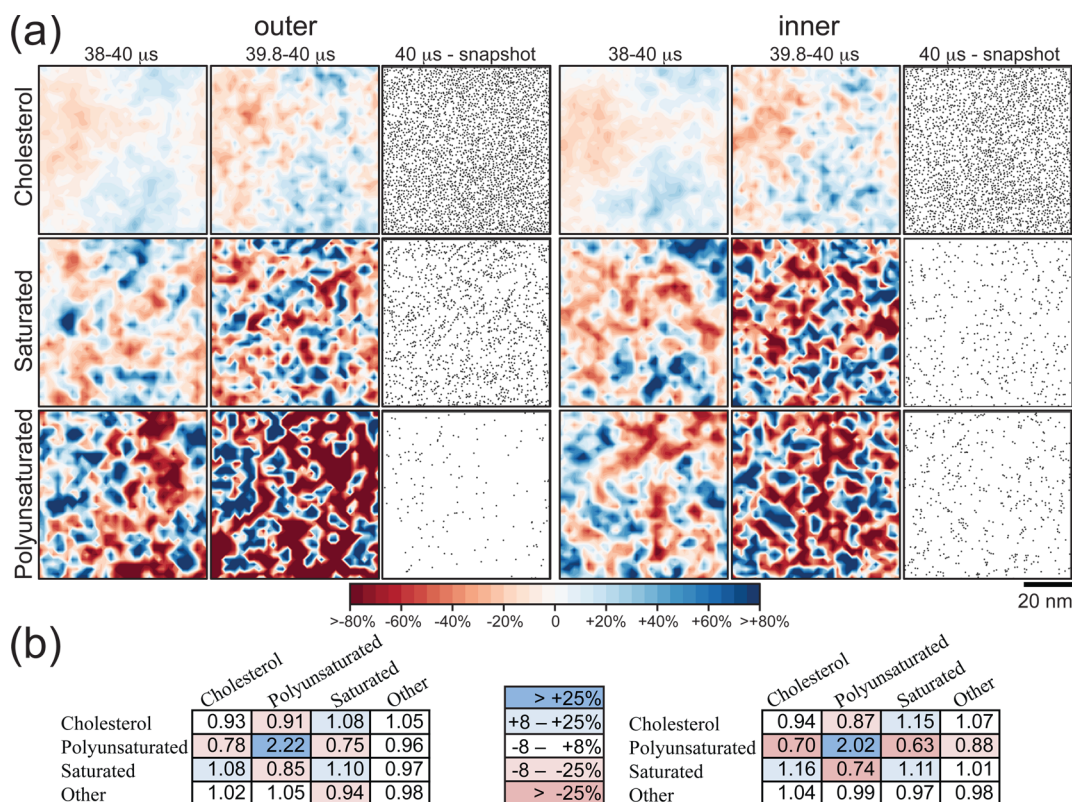


**Figure 2.** Transient plasma membrane domains. In the PM the lipids are heterogeneously mixed. (a) 2D density maps for cholesterol and saturated (both tails) and polyunsaturated lipids (both tails with 3–6 double bonds) in the plane of the bilayer; averaged over the last 2  $\mu\text{s}$ , 200 ns, and from the final snapshot only. The density maps are colored by relative enrichment (blue) or depletion (red). (b) Number of neighboring lipids (within 1.5 nm) for the last 2  $\mu\text{s}$  of the simulation. Values are normalized to the weighted average number of neighbors of each type to highlight the relative enrichment/depletion of those lipids, and boxes are colored to highlight stronger enrichment/depletion. The errors for all counts are <0.01 except for polyunsaturated vs polyunsaturated which is 0.07, see Table S5 for unnormalized counts with detailed errors.

the inner leaflet and the glycolipids (GM) in the outer leaflet. The zwitterionic lipids PC, PE, and SM are present in both leaflets, with PC and SM primarily in the outer leaflet (70%) and PE in the inner leaflet (80%). A few of the more prominent minor species were also included: ceramide (CER), diacylglycerol (DAG), lysophosphatidylcholine (LPC), with all the LPC in the inner leaflet and CER, and DAG primarily in the outer leaflet (60–65%). A total of 63 different lipid species were created by combining the lipid headgroup with various fatty acid tails, dependent on their relative prevalence.<sup>22,24–27</sup> Table S2 lists all the lipids used and their relative abundance in the inner/outer PM leaflets. The lipid tails include fatty acids from palmitoyl to lignoceroyl (16–24 carbons), and the level of saturation was varied from fully saturated to unsaturated palmitoleic acid and oleic acid tails all the way to polyunsaturated arachidonic acid and docosahexaenoic acid tails. The cholesterol concentration was 30 mol % in the main PM model and 40 mol % in an additional control model.

**Force Fields.** The Martini biomolecular CG model<sup>21,28,29</sup> was used throughout this study. Details on the lipid topologies used can be found in the Supporting Information, Force Fields section, and all the lipid parameters are available on the Martini portal, <http://cgmartini.nl/>. The Martini force field has been tested and successfully used in a large variety of lipid membrane simulations and has been shown to reproduce experimental data and all-atom simulation data across a broad range of lipid membrane properties (recently reviewed in ref 30). In particular, lipid phase diagrams are well reproduced with Martini, including liquid-ordered/liquid-disordered (Lo/Ld) phase coexistence in ternary mixtures of dipalmitoyl-PC/dilinoleyl-PC/cholesterol<sup>31,32</sup> and dioleoyl-PC/SM/cholesterol (Arnarez et al., unpublished) as well as formation of GM1 nanodomains.<sup>18</sup> Phase segregation in mixtures of dipalmitoyl-PC/dioleoyl-PC/cholesterol is only observed at reduced temperature (<290 K), which can be

attributed to the lower melting temperature  $T_m = 295$  K of dipalmitoyl-PC lipids in the Martini model compared to experiment  $T_m = 315$  K, as shown in ref 33. Note, the current PM model does not contain dipalmitoyl-PC lipids.

**Simulations.** Simulations were executed using the GROMACS simulation package version 4.5.x and 4.6.x<sup>34</sup> with the standard Martini v2.1 simulation settings.<sup>21</sup> Details on simulation setup are provided in the Supporting Information, Methods section. In short, all simulations were built using the INSANE (INSert membrANE) CG building tool. Membranes were solvated with ample water (>15 CG waters per lipid, corresponding to 60 real waters per lipid) plus counterions and 150 mM NaCl. After initial energy minimization and equilibrium runs all subsequent simulations were performed with a 20 fs time step, a temperature of 310 K set using the Bussi et al.<sup>35</sup> velocity rescaling thermostat, and a semi-isotropic pressure of 1 bar maintained with a Parrinello–Rahman barostat.<sup>36</sup>

The main PM simulation has ~20,000 lipids, ~300,000 CG water beads, ~6000  $\text{Na}^+$  and ~3200  $\text{Cl}^-$ , totaling over half a million particles in a box of  $71 \times 71 \times 11$  nm and was simulated for 40  $\mu\text{s}$ . Table S2 lists the quantity of each lipid type present and their respective ratios in the two leaflets. Figure S1 shows equilibration of the area per lipid and the total potential energy within the first 5  $\mu\text{s}$  of the simulation. To check reproducibility of our results, a series of smaller simulations were used (replicas with the same asymmetric lipid composition, with 40 mol % cholesterol, with improved treatment of water and electrostatics, and with the inner and outer leaflet mixtures setup as symmetrical bilayers, see Supporting Information, Methods section). All demonstrated similar overall characteristics as the larger PM simulation, see Figure S4 and Supporting Information, Methods section. In all simulations large-scale bilayer undulations were limited using weak Z-direction position restraint on some of the lipids in the outer leaflet, mimicking the effect of a cytoskeleton network

underpinning real plasma membranes. We verified that these constraints did not influence our results, see Figure S7 and Supporting Information, Methods section. To attain the correct cholesterol ratio between the two leaflets, based on cholesterol's chemical potential in the two leaflets, the PM simulation cholesterol distribution was iteratively varied until the initial cholesterol ratio remained stable throughout, see and Supporting Information, Methods section. The last 200 ns or 2  $\mu$ s of each simulation were used for analysis, unless otherwise specified; see Supporting Information, Methods section for details on all analysis methods.

## RESULTS AND DISCUSSION

**Outer Leaflet More Ordered and Moderately Enriched in Cholesterol.** Given the importance of cholesterol in mammalian cells, a key question to address is to what extent cholesterol is enriched in either the outer or inner leaflet. The outer leaflet of the PM contains fewer polyunsaturated and more saturated lipid tails than the inner leaflet, in particular the longer saturated tails of SM lipids. Therefore, it has been proposed that the outer leaflet contains more cholesterol.<sup>1</sup> However, the fast flip-flop rate of cholesterol has posed a challenge for determining its distribution, and some experiments have even suggested cholesterol enrichment in the inner leaflet.<sup>11,37</sup> Here we used cholesterol's fast flip-flop rate to our advantage and allowed it to redistribute between the leaflets (see Supporting Information for details). Our PM simulation shows that cholesterol distributes asymmetrically between the two leaflets with 46% and 54%  $\pm$  0.2% (SD) of the total cholesterol in the inner and outer leaflet, respectively (Figure 1c). Taking into account the different number of lipids in the two leaflets and the small proportion of cholesterol in the middle of the bilayer, the cholesterol/lipid mole fraction in the inner and outer leaflets is 0.28 and 0.31, respectively (Figure 1c and Table S2), implying a moderate but significant enrichment of cholesterol in the outer leaflet.

Together with the lower degree of unsaturation, the slight increase in cholesterol concentration makes the outer leaflet overall more ordered and better packed. The average area per lipid is  $0.513 \pm 0.001/0.553 \pm 0.001$  nm<sup>2</sup>, and global tail order is  $0.431 \pm 0.002/0.357 \pm 0.002$  for the outer/inner leaflets (see Supporting Information for details). The PM simulation provides interesting information on individual lipid types as well. For instance, polyunsaturated lipids are less ordered in the outer leaflet compared to identical lipids in the inner leaflet (Table S3). We attribute this to the inhomogeneous mixing of the polyunsaturated lipids in the plane of the membrane, see below. Lipid diffusion rates are significantly faster in the inner leaflet. The average diffusion constants for the outer and inner leaflet lipids are  $3.0 \pm 0.1$  and  $4.3 \pm 0.1 \times 10^{-7}$  cm<sup>2</sup> s<sup>-1</sup>, respectively. Saturated sphingosine lipids are the least mobile, and in particular gangliosides diffuse at less than half the rate of the other lipids (Table S4).

The rate of cholesterol flip-flop in the PM is comparable to that measured previously in simulations of fully saturated single component bilayers and somewhat slower than that in polyunsaturated bilayers.<sup>38</sup> A typical time trace of individual cholesterol flip-flop events is shown in Figure 1d. The rate of lipid flip-flop was assessed for all the PM lipids. On the time scale of the PM simulation, 40  $\mu$ s, in addition to cholesterol, only CER and DAG flip-flopped (Figure S1); DAG flip-flop rates are 2 orders of magnitude faster than CER, in overall agreement with experimental observations<sup>39</sup> (see Supporting Information, Methods section for details, flip-flop rates, and comparison to experiments).

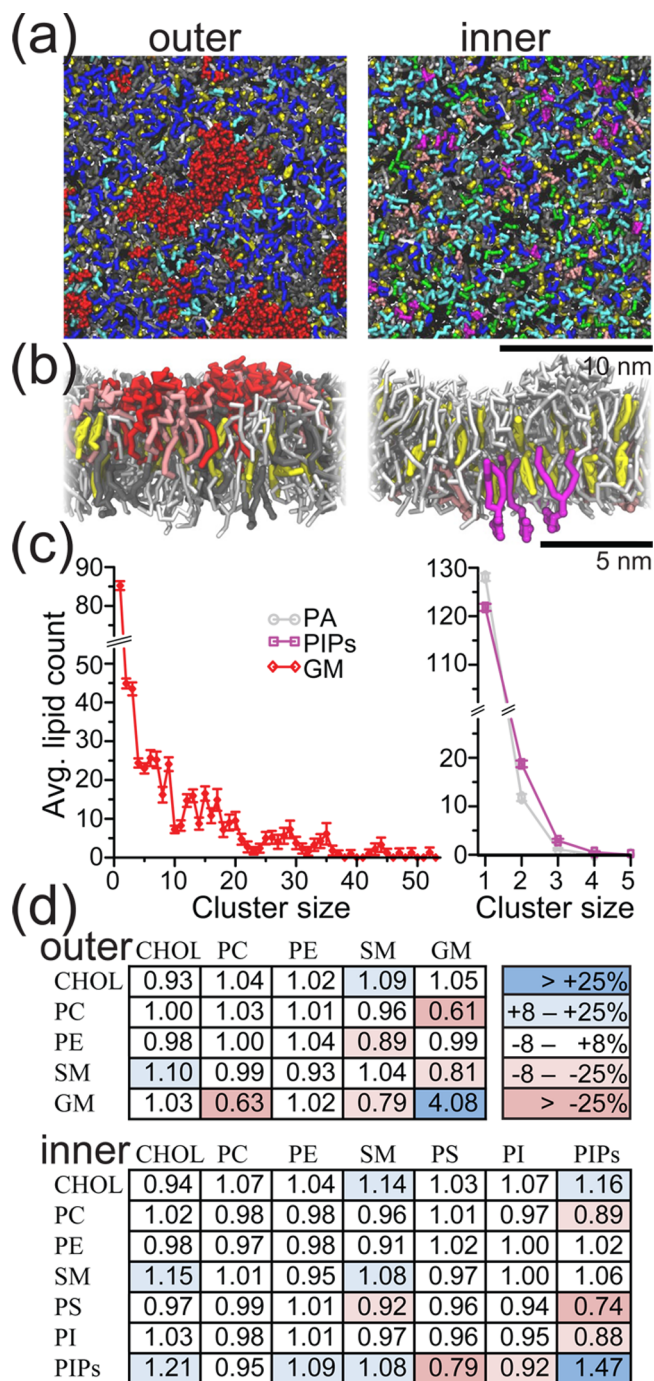


**Figure 3.** Plasma membrane organization at the headgroup level. (a) Zoomed in snapshots of the inner/outer leaflet of the PM after 40  $\mu$ s of simulation. The color scheme illustrating the mix of lipid headgroups is the same as in Figure 1. (b) Side view of the PM outer/inner surface, demonstrating the clustering of the GMs and PIPs. For clarity all lipids except for GM1 (red), GM3 (pink), SM (gray), and cholesterol (yellow) for the outer and PIPs (purple), PI (pink) and cholesterol (yellow) for the inner leaflet are drawn in light gray. (c) Showing average number of lipids present in clusters of different sizes for GM (red), PA (gray), and PIPs (purple). Values are averaged over the last 2  $\mu$ s of the simulation and error bars are s.e. GMs show high levels of clustering and PIPs moderate levels. PAs do not cluster but are shown for comparison to the PIPs, as the two groups have similar number of lipids. (d) Number of neighboring lipids (within 1.5 nm) for the last 2  $\mu$ s of the simulation. Values are determined as in Figure 2b. Errors for all counts are <0.02%, see Table S5 for unnormalized counts with detailed errors.

**Heterogeneous Lipid Mixing on Multiple Length and Time Scales.** Snapshots of the global lipid organization of the inner and outer leaflet reveal a rather homogeneous mixture, at the level of both the heads and the tails (Figure S2). To quantify the extent to which the lipids are mixed in our PM model, we calculated the average number of neighbors for different lipid types as well as density maps (see Supporting Information, Methods section). The lateral density maps of cholesterol and saturated and polyunsaturated lipids, averaged across different time windows, are shown in Figure 2, together with the preferred neighbors of these groups. Density maps and neighbor matrices of other components can be found in Figure S3 and Table S5. In addition to cholesterol asymmetrically distributing between the leaflets, cholesterol also inhomogeneously distributes in the plane of the bilayer, forming patches with slightly increased or decreased cholesterol densities. The regions of higher cholesterol density correlate with regions enriched in saturated lipids and with regions depleted in polyunsaturated lipids (Figure 2). To a lesser extent, they also correlate with higher density of ceramide-based lipids and lower density of glycerol-based lipids (Figure S3). Lipid tails also show a non-uniform distribution; in particular, longer saturated chains have reduced contacts with polyunsaturated chains. Both form veins often only a few lipids wide. A similar lateral organization is observed in multiple smaller PM control simulations and in symmetrical simulations with either inner or outer PM leaflet lipid mixture (Figure S4).

Formation of lower/higher density cholesterol regions is initiated early in the simulation (Video S1) and starts out independently in both leaflets. After a few microseconds, the domains grow in size and become correlated between leaflets. This clear co-localization (see Figures 2 and S3–S4) indicates the existence of lipid cross-talk between leaflets<sup>40,41</sup> and underlines its importance even at the microsecond time scale. As a consequence of the coupling, the membrane is somewhat thicker in regions with higher cholesterol concentration (Figure S5a). At the same time, these regions exhibit higher average tail order and slower lipid lateral diffusion (Figure S5), consistent with a liquid-ordered (Lo) phase. Conversely, the low cholesterol regions resemble a liquid-disordered (Ld) phase. However, the cholesterol enriched domains in the PM do not arise from macroscopic Lo/Ld phase separation, as seen in model membrane systems,<sup>42,43</sup> but are rapidly fluctuating and constantly forming and disappearing. The transient nature of the domains is evident from monitoring their time dependency (Video S1). Moreover, the difference in cholesterol composition between the domains only varies  $\sim 20\%$ , and domains are barely visible from instantaneous snapshots (Figure 2). Cross-correlation of the cholesterol density (Figure S9a) shows strong correlations extending up to  $15.9 \pm 2.7$  (SD) nm and  $15.5 \pm 2.5$  (SD) nm for outer and inner leaflets, respectively, and weaker correlations existing across the entire length of the simulation cell (70 nm). Time correlation of the same data (Figure S9b) reveals a non-exponential decay for  $t < 1 \mu\text{s}$ , suggestive of the presence of a hierarchy of submicrosecond time scales. The long time behavior is dominated by a single decay, however, with a correlation time of the order of  $5 \mu\text{s}$  (see Supporting Information). We attribute this time scale to the reorganization of ganglioside clusters, see below.

The lipid organization emerging from our simulations strongly resembles that of critical fluctuations as observed in real plasma membrane extracts near physiological temperature,<sup>6</sup> suggesting that the compositions of mammalian plasma

membranes are tuned to reside near a miscibility critical point. In such a case, and as observed in our simulations, domains form on a hierarchy of length and time scales.

#### Nanodomains Formed by Gangliosides and PIPs.

Gangliosides form nanodomains by themselves, both *in vitro* and *in vivo*.<sup>44,45</sup> Consistent with this data the gangliosides monosialotetrahexosylganglioside (GM1) and monosialodihexosylganglioside (GM3) show the highest non-ideal mixing behavior of all the lipids in our *in silico* model (Figure 3). Snapshots of the simulation reveal the presence of multiple ganglioside clusters, and the probability to find other gangliosides as neighbors is strongly enhanced (Figures 3 and S2). Analysis of the cluster size distribution (Figures 3c and S6) reveals a broad distribution with clusters containing up to  $\sim 50$  glycolipids. Although the cluster size distribution is not yet fully equilibrated after  $40 \mu\text{s}$  simulation, the tendency of GM1 and GM3 to aggregate further has decreased (Figure S6). Notably, the GM clusters that evolve are highly dynamic, with individual clusters breaking apart and reforming on microsecond time scales (cf. Figure S9b). The ganglioside clusters are enriched in CER and DAG and depleted in PC and lysophosphatidylcholine (LPC), see Table S5, pointing to a reduction in crowding of the bulky polysaccharide headgroups by the presence of headless lipids. A close up of a typical ganglioside cluster is shown in Figure 3b.

In the inner leaflet the phosphatidylinositol phosphates PIP<sub>1</sub>, PIP<sub>2</sub>, and PIP<sub>3</sub> (PIPs) are the only lipids to cluster significantly (Figure 3c,d), despite their (poly)anionic headgroups. Control simulations with a more advanced treatment of the electrostatic interactions confirm this result (Figure S4). PIP cluster sizes are limited to primarily dimers and trimers (Figure 3c) and corroborate recent experimental data showing the existence, in model membranes, of small (nanometer) size clusters of PIP<sub>2</sub>.<sup>46</sup> Note, the concentration of PIPs in the inner leaflet of our PM model is about 1.5 mol %. Larger PIP clusters may be present *in vivo* when PIP concentration is upregulated under specific signaling conditions.

## CONCLUSIONS

We obtained a detailed molecular view of the lipid organization of an idealized mammalian plasma membrane. The complex asymmetrical PM lipid mixture establishes an asymmetrical distribution of cholesterol, favoring the outer leaflet as well as a hierarchical lateral organization characterized by compositional fluctuations with length scales spanning the entire box and nano- to microsecond time scales. That is, the PM model shows no clear phase separation or domain formation, but the lipids are nonetheless very heterogeneously mixed. The large data set we created, including detailed characterization of the order, diffusion rates, and local environment for a broad class of PM lipids, provides insight on the functional role of different types of lipids. At the same time, our study enables a large variety of new computational studies on realistic cellular membranes. In particular, membrane proteins should be embedded, as membrane proteins occupy a significant fraction of the PM area and influence the overall PM structure and function in a fascinating lipid–protein interplay.<sup>4,5,47</sup>

## ASSOCIATED CONTENT

### Supporting Information

Supplementary methods, providing details on the force field, simulation protocols, and analysis as well as additional figures showing the plasma membrane simulation equilibrium, lipid

non-ideal mixing, repeat simulations, plasma membrane domain properties, lipid clustering, affects of suppressing bilayer undulations, and cholesterol mixing. Tables listing the plasma membrane tail distribution, lipid composition, lipid average order and diffusion, and lipid neighbors counts. Video of cholesterol non-ideal mixing time evolution. This material is available free of charge via the Internet at <http://pubs.acs.org>.

## AUTHOR INFORMATION

### Corresponding Author

s.j.marrink@rug.nl

### Notes

The authors declare no competing financial interest.

## ACKNOWLEDGMENTS

We would like to thank Prof. Gerald Feigenson for helpful discussions on finetuning the composition of our PM model. H.I.I. and M.N.M. were supported by a Rubicon and VENI (722.013.010) grant, respectively, from The Netherlands Organization for Scientific Research (NWO), and by the BE-Basic Foundation. S.J.M. and X.P. are supported by a TOP and ECHO grant from NWO. D.P.T. is an Alberta Innovates Health Solutions Scientist and Alberta Innovates Technology Futures Strategic Chair in (Bio)Molecular Simulation. Work in his group is supported by the Natural Sciences and Engineering Research Council of Canada. Computer access was granted from the National Computing Facilities Foundation (NCF) through NWO.

## REFERENCES

- (1) van Meer, G.; Voelker, D. R.; Feigenson, G. W. *Nat. Rev. Mol. Cell Biol.* **2008**, *9*, 112–124.
- (2) Sampaio, J. L.; Gerl, M. J.; Klose, C.; Ejsing, C. S.; Beug, H.; Simons, K.; Shevchenko, A. *Proc. Natl. Acad. Sci. U.S.A.* **2011**, *108*, 1903–1907.
- (3) Klose, C.; Surma, M. A.; Simons, K. *Curr. Opin. Cell Biol.* **2013**, *25*, 406–413.
- (4) Engelman, D. M. *Nature* **2005**, *438*, 578–580.
- (5) Lingwood, D.; Simons, K. *Science* **2010**, *327*, 46–50.
- (6) Veatch, S. L.; Cicuta, P.; Sengupta, P.; Honerkamp-Smith, A.; Holowka, D.; Baird, B. *ACS Chem. Biol.* **2008**, *3*, 287–293.
- (7) Baumgart, T.; Hammond, A. T.; Sengupta, P.; Hess, S. T.; Holowka, D. A.; Baird, B. A.; Webb, W. W. *Proc. Natl. Acad. Sci. U.S.A.* **2007**, *104*, 3165–3170.
- (8) Kaiser, H.-J.; Lingwood, D.; Levental, I.; Sampaio, J. L.; Kalvodova, L.; Rajendran, L.; Simons, K. *Proc. Natl. Acad. Sci. U.S.A.* **2009**, *106*, 16645–16650.
- (9) van Meer, G. *EMBO J.* **2005**, *24*, 3159–3165.
- (10) Holthuis, J. C. M.; Menon, A. K. *Nature* **2014**, *510*, 48–57.
- (11) Devaux, P. F.; Morris, R. *Traffic* **2004**, *5*, 241–246.
- (12) Eggeling, C.; Ringemann, C.; Medda, R.; Schwarzmann, G. *Nature* **2009**, *457*, 1159–1162.
- (13) Lee, E. H.; Hsin, J.; Sotomayor, M.; Comellas, G.; Schulten, K. *Structure* **2009**, *17*, 1295–1306.
- (14) Dror, R. O.; Dirks, R. M.; Grossman, J. P.; Xu, H.; Shaw, D. E. *Annu. Rev. Biophys.* **2012**, *41*, 429–452.
- (15) Marrink, S. J.; de Vries, A. H.; Tieleman, D. P. *Biochim. Biophys. Acta* **2009**, *1788*, 149–168.
- (16) Vacha, R.; Berkowitz, M. L.; Jungwirth, P. *Biophys. J.* **2009**, *96*, 4493–4501.
- (17) Wu, E. L.; Fleming, P. J.; Yeom, M. S.; Widmalm, G.; Klauda, J. B.; Fleming, K. G.; Im, W. *Biophys. J.* **2014**, *106*, 2493–2502.
- (18) de Jong, D. H.; Lopez, C. A.; Marrink, S. J. *Faraday Discuss.* **2013**, *161*, 347–363.
- (19) Jo, S.; Lim, J. B.; Klauda, J. B.; Im, W. *Biophys. J.* **2009**, *97*, 50–58.

- (20) Mouritsen, O. G.; Zuckermann, M. J. *Lipids* **2004**, *39*, 1101–1113.
- (21) Marrink, S. J.; Risselada, H. J.; Yefimov, S.; Tieleman, D. P.; De Vries, A. H. *J. Phys. Chem. B* **2007**, *111*, 7812–7824.
- (22) Han, X.; Gross, R. W. *Proc. Natl. Acad. Sci. U.S.A.* **1994**, *91*, 10635–10639.
- (23) Virtanen, J. A.; Cheng, K. H.; Somerharju, P. *Proc. Natl. Acad. Sci. U.S.A.* **1998**, *95*, 4964–4969.
- (24) Dodge, J. T.; Phillips, G. B. *J. Lipid Res.* **1967**, *8*, 667–675.
- (25) Fridriksson, E. K.; Shipkova, P. A.; Sheets, E. D.; Holowka, D.; Baird, B.; McLafferty, F. W. *Biochemistry* **1999**, *38*, 8056–8063.
- (26) Pike, L. J.; Han, X.; Chung, K. N.; Gross, R. W. *Biochemistry* **2002**, *41*, 2075–2088.
- (27) Gerl, M. J.; Sampaio, J. L.; Urban, S.; Kalvodova, L.; Verbavatz, J. M.; Binnington, B.; Lindemann, D.; Lingwood, C. A.; Shevchenko, A.; Schroeder, C.; Simons, K. *J. Cell Biol.* **2012**, *196*, 213–221.
- (28) Marrink, S. J.; De Vries, A. H.; Mark, A. E. *J. Phys. Chem. B* **2004**, *108*, 750–760.
- (29) Monticelli, L.; Kandasamy, S. K.; Periole, X.; Larson, R. G.; Tieleman, D. P.; Marrink, S. J. *J. Chem. Theory Comput.* **2008**, *4*, 819–834.
- (30) Marrink, S. J.; Tieleman, D. P. *Chem. Soc. Rev.* **2013**, *42*, 6801.
- (31) Risselada, H. J.; Marrink, S. J. *Proc. Natl. Acad. Sci. U.S.A.* **2008**, *105*, 17367–17372.
- (32) Domański, J.; Marrink, S. J.; Schäfer, L. V. *Biochim. Biophys. Acta* **2012**, *1818*, 984–994.
- (33) Marrink, S. J.; Risselada, J.; Mark, A. E. *Chem. Phys. Lipids* **2005**, *135*, 223–244.
- (34) Hess, B.; Kutzner, C.; van der Spoel, D.; Lindahl, E. *J. Chem. Theory Comput.* **2008**, *4*, 435–447.
- (35) Bussi, G.; Donadio, D.; Parrinello, M. *J. Chem. Phys.* **2007**, *126*, 014101.
- (36) Parrinello, M.; Rahman, A. *J. Appl. Phys.* **1981**, *52*, 7182–7190.
- (37) Mondal, M.; Mesmin, B.; Mukherjee, S.; Maxfield, F. R. *Mol. Biol. Cell* **2009**, *20*, 581–588.
- (38) Bennett, W. F. D.; MacCallum, J. L.; Hinner, M. J.; Marrink, S. J.; Tieleman, D. P. *J. Am. Chem. Soc.* **2009**, *131*, 12714–12720.
- (39) Bai, J.; Pagano, R. E. *Biochemistry* **1997**, *36*, 8840–8848.
- (40) Kiessling, V.; Crane, J. M.; Tamm, L. K. *Biophys. J.* **2006**, *91*, 3313–3326.
- (41) Collins, M. D.; Keller, S. L. *Proc. Natl. Acad. Sci. U.S.A.* **2008**, *105*, 124–128.
- (42) Baumgart, T.; Hess, S. T.; Webb, W. W. *Nature* **2003**, *425*, 821–824.
- (43) Heberle, F. A.; Petruziello, R. S.; Pan, J.; Drazba, P.; Kučerka, N.; Standaert, R. F.; Feigenson, G. W.; Katsaras, J. *J. Am. Chem. Soc.* **2013**, *135*, 6853–6859.
- (44) Prinetti, A.; Loberto, N.; Chigorno, V.; Sonnino, S. *Biochim. Biophys. Acta* **2009**, *1788*, 184–193.
- (45) Westerlund, B.; Slotte, J. P. *Biochim. Biophys. Acta* **2009**, *1788*, 194–201.
- (46) Salvemini, I. L.; Gau, D. M.; Reid, J.; Bagatolli, L. A.; Macmillan, A.; Moens, P. D. *J. Chem. Phys. Lipids* **2014**, *177*, 51–63.
- (47) Laganowsky, A.; Reading, E.; Allison, T. M.; Ulmschneider, M. B.; Degiacomi, M. T.; Baldwin, A. J.; Robinson, C. V. *Nature* **2014**, *510*, 172–175.